Supporting Online Information for

Nanoscale Plasmonic Interferometers for Multi-Spectral, High-Throughput Biochemical Sensing

*Jing Feng[(a)], Vince S. Siu[(a)], Alec Roelke, Vihang Mehta, Steve Y. Rhieu, G. Tayhas R. Palmore, and Domenico Pacifici**

School of Engineering, Brown University, Providence, Rhode Island 02912.

(a) These authors have contributed equally to the experimental work reported in the paper.

* Corresponding author: Domenico_Pacifici@brown.edu

Supporting Information Contents

1. Fabrication and structural characterization of groove-slit and groove-slit-groove plasmonic interferometers

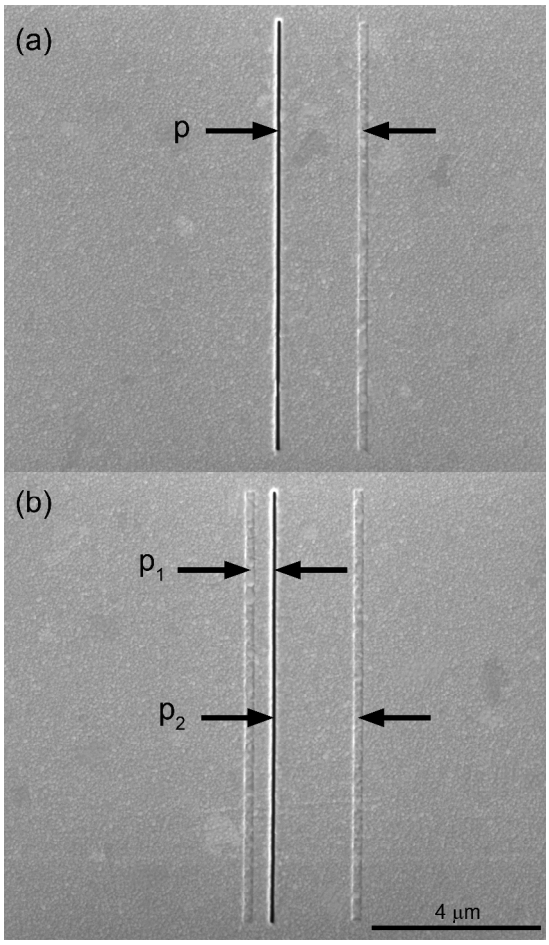

Figure S1. Scanning electron microscopy (SEM) images of two different types of plasmonic interferometers: (a) a groove-slit plasmonic interferometer with interferometer arm (groove-slit separation distance) p = 2.00 μm, (b) a groove-slit-groove plasmonic interferometer with p_1 = 0.57 μm and p_2 = 2.00 μm. The groove width is 200 nm, length is 10 μm and depth is ~20 nm. The slit is 100 nm wide, 10 μm long and 300 nm deep.

Plasmonic interferometers consisting of groove-slit (GS) and groove-slit-groove (GSG) structures were fabricated in a metal film by focused ion beam milling. Using electron beam evaporation, a 4-nm-thick titanium adhesion layer was first deposited onto previously cleaned quartz slides, followed by a 300-nm-thick silver layer. Silver was chosen because it supports SPPs that can propagate for several tens of micrometers without significant attenuation, allowing fabrication of plasmonic interferometers with arm length ranging between ~ 200 nm – 20μm. Plasmonic interferometers were then fabricated using focused ion beam (FIB) milling, with a

typical Ga-ion beam current of 200 pA and an accelerating voltage of 30 kV. By using a custom made scripting routine able to automatically move the sample stage, adjust beam focus and stigmatism at each sample location, and etch the devices with specified width, length and interferometer arm length, more than 1,000 plasmonic interferometers can be milled in less than two hours, over an area of ~ 1 mm^2. Several columns of GSG devices were milled according to various combinations of interferometer arm lengths with p_1 (left groove-slit separation distance) held constant to 0.4, 0.57, 0.74, 0.89, 1.09, 1.67 and 5.70 μm, respectively for each column, and p_2 (right slit-groove distance) varying from 0.25 to 10 μm increasing in steps of 25 nm. The interferometer arm lengths have been chosen based on optimized sensitivity and sensor response as simulated using the model developed in the following. For comparison, a single column of GS devices was also milled on the same chip (Fig. S1).

The spectral dependence of light intensity transmitted through the slit of each plasmonic interferometer was measured using a modified inverted microscope (Nikon Ti Eclipse) coupled to a spectrograph and a CCD camera. A 100 W broadband halogen light source was aligned to the optical axis of the inverted microscope. For the experiment, both the field and aperture diaphragms of the microscope condenser lens were closed to achieve a collimated light beam, normally incident upon the top of the sample surface, as schematically shown in Fig. 1(b). An actual power density of only 10^{-2} W/cm^2 incident on the sample was measured by a calibrated photo diode (integrated over the full wavelength range). The low power density and continuous flow of water employed during the sensing experiment allowed the temperature of the device to be held constant throughout the experiment. The far-field light intensity transmitted through the slit of each plasmonic interferometer was then collected by a 40× objective lens with numerical aperture NA = 0.6, dispersed using a single-grating monochromator and detected with a CCD camera. Spectral resolution of our set-up was ~0.4 nm; the number of counts and acquired spectra per experiment were adjusted to ensure a statistical error of <0.1% in the measured transmitted intensity.

2. Simulated transmission spectra (normalized to single slit) for groove-slit and groove-slit-groove plasmonic interferometers

Figure S2 shows simulated light intensity transmitted through the slit of a groove-slit-groove (black line) and a groove-slit (red line) plasmonic interferometer on a Ag/water interface. These two plasmonic interferometers share a constant groove-slit distance equal to 0.57 μm, which causes the envelope profile (red line) in their normalized transmission spectra. As mentioned in the main text, the groove-slit-groove plasmonic interferometer has a greater number and sharper maxima and minima due to the "three-beam interference" (i.e. incident beam and two counter-propagating SPPs interfering at the slit location) caused by the addition of an extra groove that defines a second arm in the plasmonic interferometer. Therefore, groove-slit-groove plasmonic interferometers will be more sensitive for sensing applications, thanks to smaller full width at half maxima (FWHM) compared to a groove-slit plasmonic interferometer.

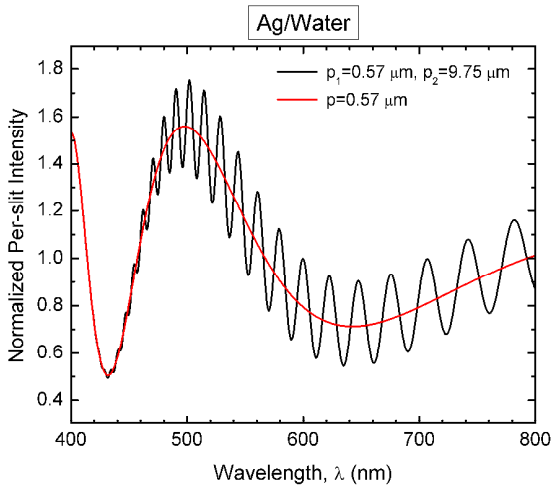

Figure S2. Simulated normalized per-slit transmitted intensity spectra for a two-arm plasmonic interferometer with two grooves at distances of p_1 = 0.57 μm and p_2 = 9.75 from the slit (black line), a one-arm plasmonic interferometer with one groove p = 0.57 μm (red line).

3. Color map of experimental transmission spectra (normalized to single slit) for groove-slit plasmonic interferometers as a function of wavelength λ and groove-slit distance p

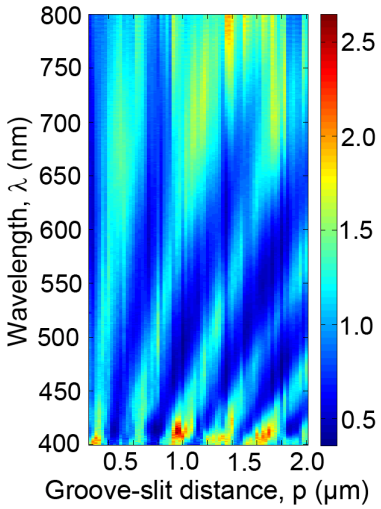

Figure S3. 2D experimental color map of normalized to single-slit light intensity transmitted through the slits of several groove-slit plasmonic interferometers, as a function of groove-slit distance p and wavelength λ (Ag/air interface).

4. Wavelength dependence of SPP effective excitation efficiency

According to the interference model developed in the text, the interference effect between the incident beam and the surface plasmon polaritons (SPPs) generated by the groove in a groove-slit plasmonic interferometer gives the following expression for the normalized transmitted intensity:

$$I_T / I_0 = \left|1 + \beta e^{i\phi}\right|^2 \tag{S1}$$

where β is the SPP excitation efficiency for the groove (defined as the ratio between the in-plane scattered SPP field amplitude and the incident field), which is related to the geometry of the groove (such as depth and width); ϕ is the phase shift of the SPP, dependent on the free-space wavelength, angle of incidence, groove-slit distance, scattering phase, and material properties (dielectric constants), all of which are known parameters. At a certain wavelength, if we take a horizontal cut in Fig. S3, we can obtain the normalized transmitted intensity as a function of groove-slit distance. By fitting the transmitted data, we can then determine the effective excitation efficiency β at that specific wavelength, represented as a single black dot in Fig. S4. By fitting the β values determined at wavelengths increasing in steps of 25 nm with the least-square method, we determined the relationship between effective excitation efficiency and wavelength as: $\beta = 128.2/\lambda$, with λ in nm, which has not been reported in literature to the best of our knowledge. In particular, β is ~0.3 at 460 nm and it decreases to ~0.15 at 760 nm. In principle, our technique can be employed to determine β at any wavelength, for any groove width, depth and length, or metal/dielectric combination.

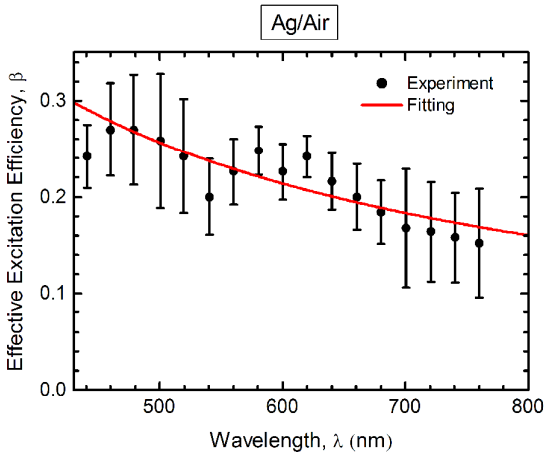

Figure S4. Wavelength dependence of the excitation efficiency β for SPPs generated by diffractive scattering by a 200-nm-wide groove milled in Ag with air as the dielectric medium. Data points were determined from the experiments of the groove-slit plasmonic interferometer with varying p (black dots). The red line is a fit of the experimentally determined data based on a least-square fitting method.

5. Color maps of simulated transmission spectra (normalized to single slit) for different dielectric materials (Ag/air: top panels, Ag/water: bottom panels)

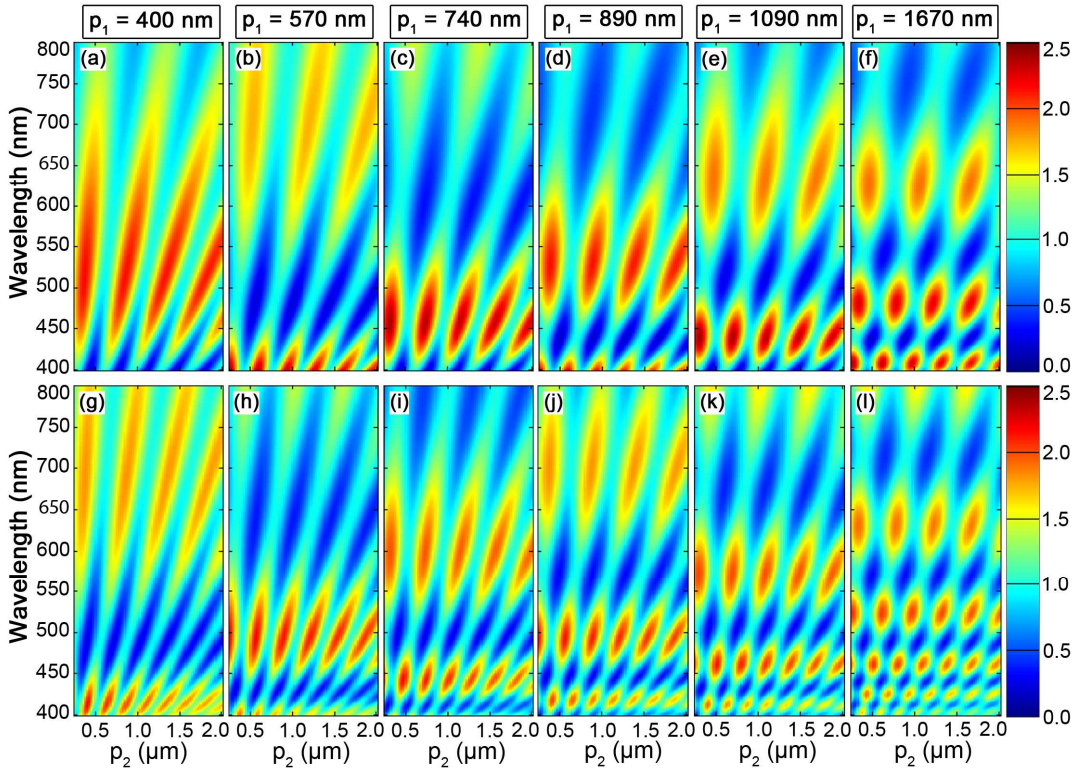

Figure S5. Simulated color maps showing normalized per-slit transmission spectra (wavelength in vertical axis) for groove-slit-groove plasmonic interferometers with fixed p_1 (400, 570, 740, 890, 1090, 1670 nm) and varying p_2 (250 - 2000 nm, in steps of 25 nm), using white light illumination incident upon a Ag/air interface ((a)-(f)) and a Ag/water interface ((g)-(l)). The dielectric constant of water at various wavelengths was used to calculate (g)-(l). It is interesting to note that the increased refractive index of water determines the appearance of more peaks (compared to air) in the color maps for the very same devices.

6. Comparison between color maps of experimental and simulated transmission spectra (normalized to single slit) versus groove-slit distance p_2 and wavelength λ, for a fixed p_1 = 0.57 μm

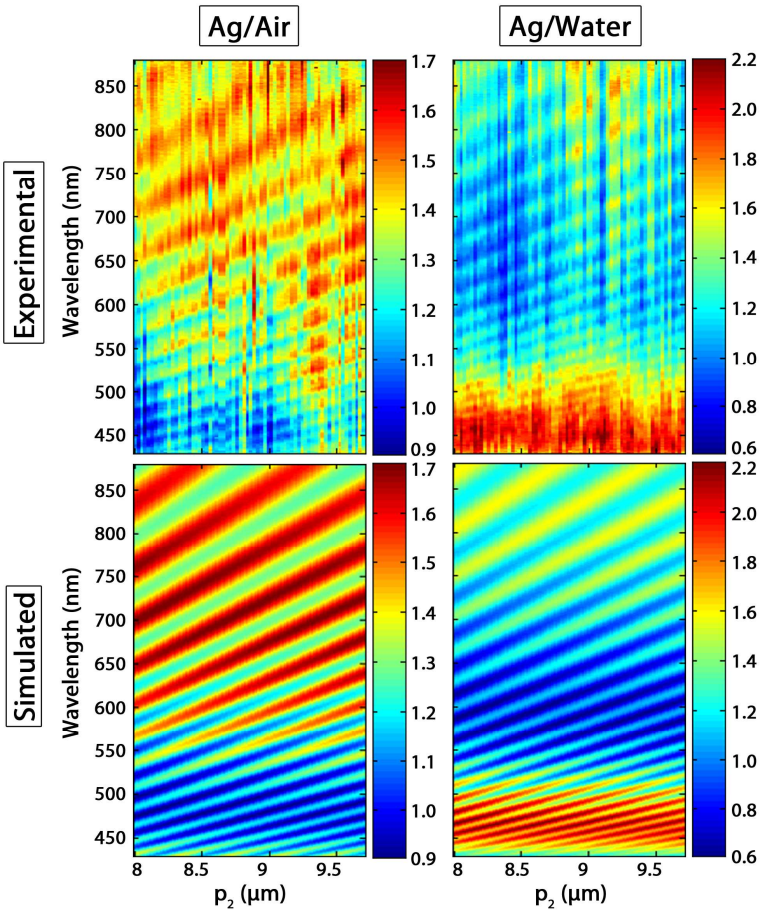

Figure S6. Color maps showing a comparison between experimental and simulated transmission spectra (normalized to single slit) for groove-slit-groove plasmonic interferometers with varying p_2 (between 8.00 - 9.70 μm) for Ag/air and Ag/water interfaces.

7. Color map of simulated transmission spectra (normalized to single slit) for groove-slit-groove interferometers with p_2 extending up to 10 μm

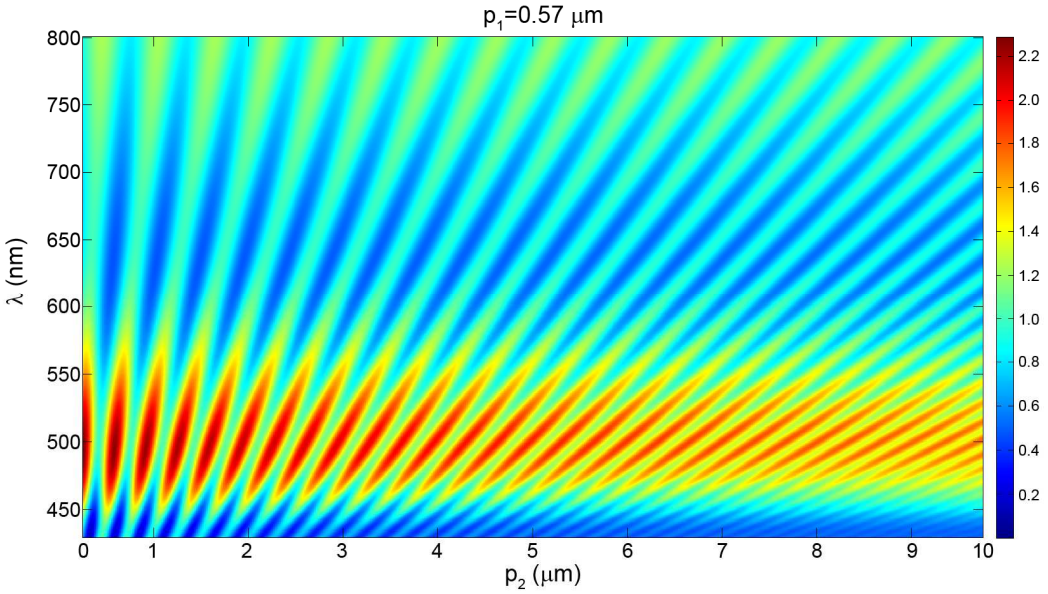

Figure S7. Color map shows simulated normalized transmission spectra (wavelength in vertical axis) for groove-slit-groove plasmonic interferometers with fixed p_1 = 0.57 μm and varying p_2 (0.25 - 10 μm, in steps of 25 nm), for a Ag/water interface. With larger p_2, there are more peaks and valleys in the spectra (vertical cuts), even for plasmonic interferometer arms as long as 10 μm, which suggests that longer plasmonic interferometers have higher sensitivity. Due to absorption losses in the metal, the amplitude of the SPPs generated by longer plasmonic interferometers is attenuated, and as a result the constructive and destructive interference effects are less pronounced. This explains the lower values of per-slit normalized transmission maxima observed at p_2 = 10 μm.

8. Fabrication of the microfluidic channel

A 1” by 1” quartz master was created by patterning SU-8 negative photoresist (MicroChem Corporation, Newton, MA) into a rectangular microchannel with dimensions of 2-cm long × 1-cm wide × 70-μm high. Polydimethylsiloxane (PDMS) pre-polymer and a curing agent (SYLGARD 184 Silicone Elastomer Kit, Dow Corning, Midland, MI) were mixed in a 10:1 mass ratio, degassed using a vacuum desiccator, and cured against the master at 70 °C for 5 hours. The PDMS was peeled from the master and inlet and outlet holes were punched using a 1.2 mm hole puncher (Harris Uni-core, Ted Pella Inc.). A custom holder was created to securely sandwich the PDMS on top of the patterned quartz substrate with an array of plasmonic interferometers while allowing perfect allocation in the automated microscope stage slot.

9. Calculations of the SPP skin depth and propagation length

As we know, the field amplitude of SPPs decreases exponentially in the direction perpendicular to the metal/dielectric interface. Skin depth is the value at which the field amplitude falls to $1/e$.[1] Skin depth δ at a wavelength λ is calculated according to:

$$\delta = \frac{\lambda}{2\pi}\left(\frac{\varepsilon_{1r} + \varepsilon_2}{\varepsilon_2^2}\right)^{1/2} \tag{S2}$$

where ε_{1r} is the real part of the dielectric constant of the metal medium, and ε_2 is the dielectric constant of the dielectric medium above the metal. Figure S8(a) shows skin depth as a function of wavelength on Ag/air (red) and Ag/water (black) interfaces.

The intensity of SPPs propagating along a smooth surface also decreases exponentially because of ohmic losses in the metal. The propagation length L is the length at which the intensity decreases to $1/e$:

$$L = \frac{c}{\omega}\left(\frac{\varepsilon_{1r} + \varepsilon_2}{\varepsilon_{1r}\varepsilon_2}\right)^{3/2}\frac{\varepsilon_{1r}^2}{\varepsilon_{1i}} \tag{S3}$$

where c is the speed of light, ω is the frequency at certain free-space wavelength, and ε_{1i} is the imaginary part of the dielectric constant of the metal medium. Figure S8(b) shows the propagation length spectra on Ag/air (red) and Ag/water (black) interfaces.

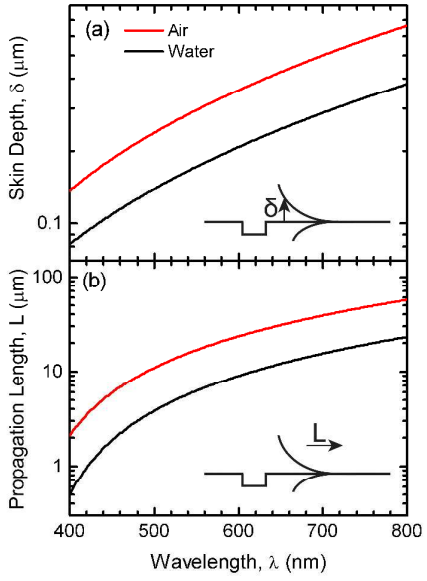

Figure S8. (a) Skin depth of SPPs as a function of wavelength on Ag/air (red line) and Ag/water (black line) interface. (b) Propagation length of SPP as a function of wavelength on Ag/air (red line) and Ag/water (black line) interface.

1. Raether, H. *Surface Plasmons on Smooth and Rough Surfaces and on Gratings*; Springer: Berlin, **1988**.

10. Calculation of the sensing volume

As we notice in Fig. S8(b), on Ag/water interface, propagation length is slightly above 10 μm at a wavelength of 800 nm. To ensure that the SPPs excited by the grooves can reach the slit location, the maximum groove-slit distance we can use is within 10 μm. Thus, in our experiment, we selected 9.75 μm as the maximum distance for p_2. The width of the sensing volume is the sum of the two groove-slit distances, p_1 and p_2. For example, taking into account a plasmonic interferometer with p_1 = 0.57 μm and p_2 = 9.75 μm, the sensing width is 10.32 μm. We assumed the sensing height is equal to the skin depth at a specified wavelength (calculated from Eqn. (S2)), since above this height little information can be delivered by the SPPs. At λ = 590 nm, the skin depth is ~200 nm at a Ag/water interface. The length of our plasmonic interferometer is 10 μm, giving a final sensing volume of 20 μm^3, i.e. 20 fL.

11. Refractive index of glucose solutions in water

Figure S9 illustrates the refractive index as a function of glucose concentration, ρ (mg/dL), at a wavelength of 589 nm at 20 °C. The index of pure water is 1.3330 at 20 °C. A second order polynomial fitting is applied and the output is

$$n = 1.333000 + 1.42382 \times 10^{-6} \rho - 5.19903 \times 10^{-13} \rho^2 \qquad \text{(S4)}$$

At a specific glucose concentration (ρ), we can calculate the refractive index of the solution by using Eq. (S4).

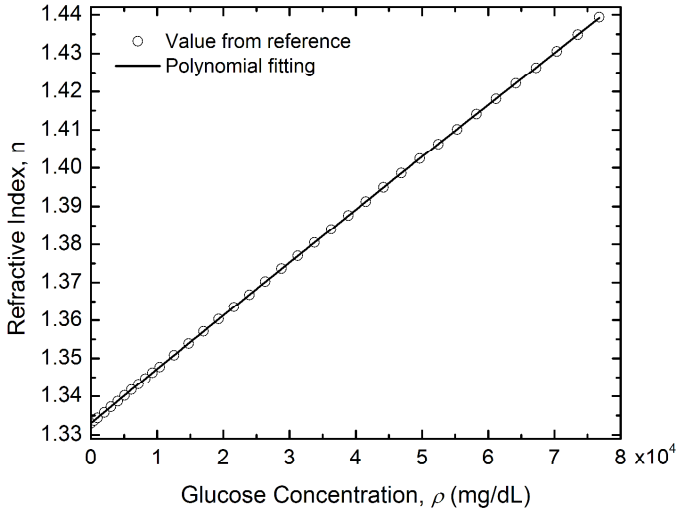

Figure S9. Refractive index as a function of glucose concentration (ρ), at a wavelength of 589 nm, 20 °C.[2]

2. Lide, D. R. *CRC Handbook of Chemistry and Physics*, 84th ed.; CRC Press: Boca Raton, FL., **2003**.

12. Simulated figure of merit (FOM_I) versus of glucose concentration and groove-slit distance p_2 at fixed λ = 590 nm and p_1 = 0.57 μm

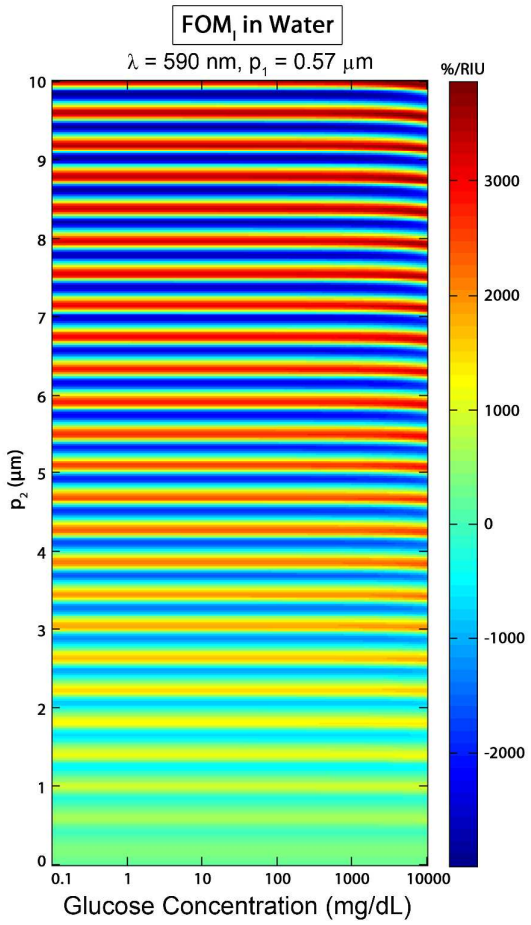

Figure S10. Color map reporting the simulated figure of merit (FOM_I) as a function of glucose concentration and groove-slit distance p_2, for a fixed wavelength λ = 590 nm and groove-slit distance p_1 = 0.57 μm. Plasmonic interferometers with longer p_2 have a higher FOM_I. However, for a given device, the FOM_I decreases at higher concentrations, as experimentally observed.

13. Simulated figure of merit (FOM_I) versus of groove-slit distances p_1 and p_2 at various glucose concentrations

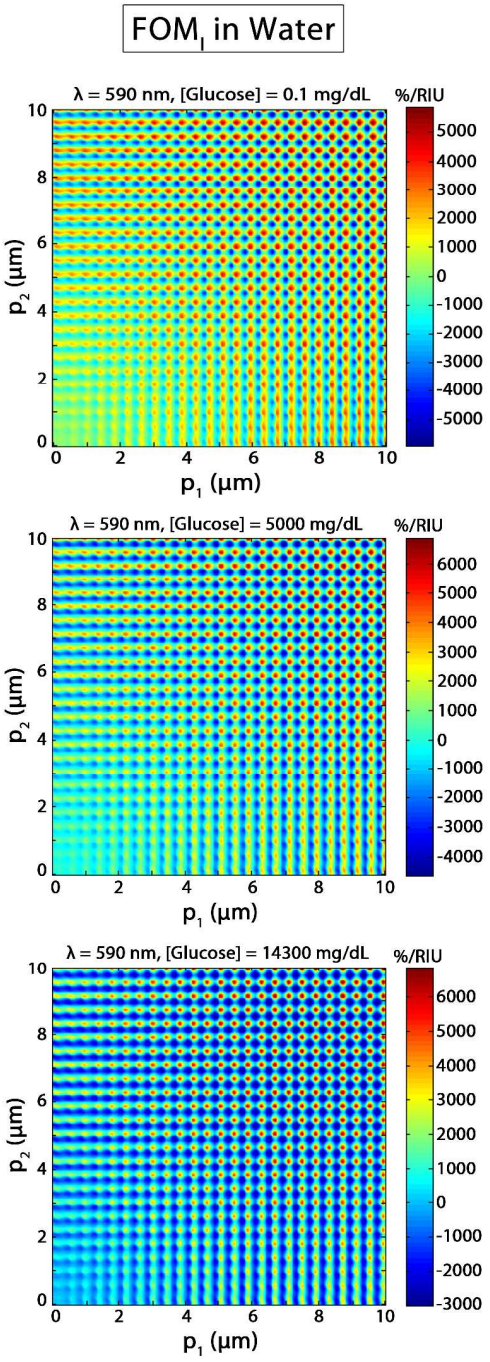

Figure S11. Color maps of simulated FOM_I as a function of groove-slit distances p_1 and p_2, for various glucose concentrations: 0.1, 5000, 14300 mg/dL.

14. Simulated figure of merit (FOM_I) versus glucose concentration for three different devices at a fixed wavelength (λ = 590 nm)

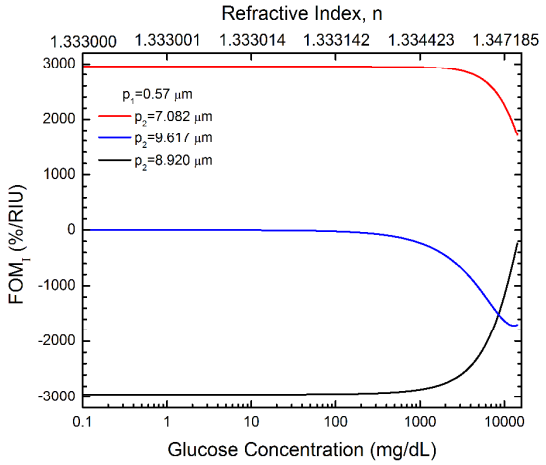

Figure S12. Plots of simulated FOM_I versus glucose concentration for three different devices, at a fixed wavelength (λ = 590 nm). The plots show the complex non-linear functional dependence of FOM_I. In particular, the blue line reports on the FOM_I of a device that shows no significant change in transmitted intensity up to a concentration of 200 mg/dL. This evidences the importance of careful choice of p_1, p_2 and λ for the optimization of device sensitivity in the concentration range of interest.